Title

Ongoing advancement of free-moving radiation imaging and mapping

Authors

Quiter, Brian J
Bandstra, Mark S
Cates, Joshua W
et al.

Publication Date

2022-10-04

DOI

10.1117/12.2635752

Peer reviewed

Ongoing advancement of free-moving radiation imaging and mapping

Brian J. Quiter[a], Mark S. Bandstra[a], Joshua W. Cates[a], Reynold J. Cooper[a], Joseph C. Curtis[a], Daniel Hellfeld[a], Tenzing H.Y. Joshi[a], Ryan T. Pavlovsky[a], Emil Rofors[a], Marco Salathe[a], Jayson R. Vavrek[a], and Kai Vetter[a,b]

[a]Lawrence Berkeley National Laboratory, 1 Cyclotron Rd., Berkeley, CA, USA
[b]University of California, Berkeley, CA, USA

ABSTRACT

By combining radiation detection technologies with robotics sensing, the ability to continuously conduct gamma-ray imaging using freely-moving systems was demonstrated in 2015.[1] This new method, which was named free-moving 3D Scene Data Fusion (SDF), was then applied to mapping radioactive contamination and to contextualizing the extent of contamination and the efficacy of radiological clean-up efforts.[2,3] Since then, further studies into the types of radiation detection systems to which SDF could be applied resulted in the discovery and demonstration that neutron activity could be mapped using neutron-sensitive CLLBC scintillators, arrays of pixelated CZT detectors could be used to create multi-modal imagers, and more rudimentary detector systems such as arrays of four CsI modules could still achieve good-quality mapping by inferring source positioning through the encoded modulation of source-to-detector distance. This paper provides an overview of the SDF technology, highlights recent measurements leveraging SDF-equipped systems, discusses the continued development of quantitative algorithms[4,5] and their ramifications for developing autonomous SDF-capabilities, and summarizes future directions of research and application development for free moving radiation detection systems.

Keywords: Radiation imaging, robotics, SPIE, Scene Data Fusion

1. INTRODUCTION

The concept of 3D Scene Data Fusion was presented at SPIE Optics+Photonics 2019.[6] In that presentation, applications of contamination mapping and finding radiological sources took center stage; the ability to image the distribution of uranium hexafloride within a container was also shown. Many of the SDF measurements that have been performed have leveraged a compact, portable platform referred to as a Localization and Mapping Platform (LAMP).[7,8] Since the 2019 presentation, LBNL has continued to develop the SDF technology by coupling the concept to new radiation detector systems, developing new methods of analyzing the radiological data, and by identifying and investigating new applications to which SDF can be applied. Many of new developments have been published elsewhere, but this paper summarizes those developments as well as highlights a few new concepts of applying the SDF technology.

2. SDF OVERVIEW

Scene data fusion, at its core, is the continuous formulation and solving of a series of coupled linear equations. The contextual sensors, made popular by robotic sensing, such as a LiDAR or visual cameras are used in conjunction with inertial measurement units to enable simultaneous localization and mapping (SLAM) algorithms such Cartographer[9] to continuously locate the position of the radiation mapping system in a growing digital rendering of the measured area (i.e., a 'map'). Within the SDF algorithm framework, the contextual map is voxelized and each voxel is considered a potential source of radioactive emanations. Instantaneous positions and orientations (at time, i) of the radiation detection system are known within this map and a *sensitivity* function, S_{iJ} is calculated for each of the voxels (indexed by j). The sensitivity function describes the probability that each

Further author information: (Send correspondence to B.J.Q.)
B.J.Q.: E-mail: bjquiter@lbl.gov, Telephone: 1 510 486 6776

specific observation of ionizing radiation by the detector system (termed an 'event' and associated with at least an energy measurement and corresponding time) could have originated from each voxel, combining sensitivity functions for each observation produces $\overleftrightarrow{S}$, the system matrix. The list of counted events, $\vec{C}$ (or a time interval of events) are then related to the emissivity within a specific energy interval of each voxel, A_j, which establishes a system of equations,

$$\vec{C} = \overleftrightarrow{S}\vec{A}. \tag{1}$$

At the time of SPIE Optics+Photonics 2019, $\overleftrightarrow{S}$ typically comprised qualitative angular efficiency relationships, $\epsilon(\Omega_{ij})$, that encoded features expected from angular dependencies - such as a cosine function for angles relative to face normals - but did not feature any rigorously determined efficiencies, thereby making the mapping results qualitative in nature. One exception was the work by Joshi et al.,[10] where despite doing so in post-processing, the authors were able to leverage experimentally measured angular efficiencies to perform the first quantitative SDF analysis using maximum likelihood expectation maximization (ML-EM) to solve Eq. 1. ML-EM had been the solver method of choice for SDF, but the work in Joshi et al. inspired more quantitative assessments and the development other quantitative algorithms. These more recent efforts will be summarized in Section 3.

Meanwhile, the SDF concept was found to not be limited to the high-fidelity gamma-ray imagers for which it was first conceived. LBNL constructed a LAMP detector array based on the CLLBC scintillator[11,12] produced by RMD Inc., which is enriched in ^{6}Li and therefore sensitive to neutrons, particularly to thermal neutrons through the n+^{6}Li $\rightarrow$ ^{4}He + ^{3}H reaction. This detector system, called NG-LAMP (due to its dual sensitivity to both neutrons and gamma rays), was demonstrated to be able to localize neutron sources in a variety of configurations. Figure 1 shows an example of NG-LAMP localizing a Pu surrogate source in the trunk of a vehicle. The source was heavily shielded by Pb and W to reduce the emitted gamma-ray flux to background levels at the exterior of the vehicle. NG-LAMP was carried on a small unmanned aerial vehicle (sUAV) and scanned the parked vehicle in less than a minute. Two separate ML-EM solutions to Eq.1 were computed and are shown in the figure. The best-fit distribution for gross gamma emissivity is shown in blue and the thermal neutron activity is shown in red. There are no high-activity gamma voxels in the reconstruction, which is consistent with the source being shielded to background levels. Conversely, the thermal neutron activity is strongly localized near the back of the vehicle. These results were first presented by Pavlovsky et al.[7]

In some environments, having good imaging fidelity as well as real-time feedback is very helpful for localizing a radioactive source and for providing an operator with understanding of a radiological environment. With the initial intention of supporting safeguards measurements such as item characterization and accountancy, LBNL developed Polaris-LAMP,[13] which comprised of the LAMP contextual sensors and computing coupled to a Polaris-H CZT-based gamma-ray imager developed by H3D.[14] This detector proved useful for identifying radioactive components of vehicles parked on the Fukushima Dai'ichi nuclear power plant site.[15]

Polaris-LAMP was also able to initially locate and attribute hold-up of ^{237}Np in an exhaust vent of a glove box at facility being prepared for demolition within the Savannah River Site H-Canyon. The glove box was part of a series of glove boxes that were used to machine ^{237}Np targets prior to irradiation for the purpose of harvesting ^{238}Pu for radioisotope thermoelectric generators for NASA.[16] As part of the decontamination effort, the front sides of the glove boxes were being imaged by SRNL researchers using overnight exposures with GeGI detectors made by PhDs Inc. to identify locations of residual ^{237}Np; however the back sides of the glove boxes had not been studied, but it was known that the radiation field was still significantly above background despite significant shielding present on the back sides of the boxes.

As part of a collaborative effort, SRNL invited LBNL researches to survey the facility with LAMP systems. Using Polaris-LAMP and a few-minute survey, LBNL was able to locate the source of significant radioactivity to an air outlet pipe on the back of one of the glove boxes. Figure 2 shows a coarse video overlay that was displayed on the LAMP user interface in real-time and the SDF data product where a perspective view of the point cloud along with the attributed activity are shown. The reconstruction was performed by Compton imaging photons with the 312-keV region that was primarily populated by ^{233}Pa radioactive decay. ^{237}Np decays to ^{233}Pa via α-particle emission.

In the SDF rendering of Figure 2, the walls in the foreground were removed for clarity, but some objects against the nearest wall remain visible in the point cloud. One of those objects is another glove box. When the

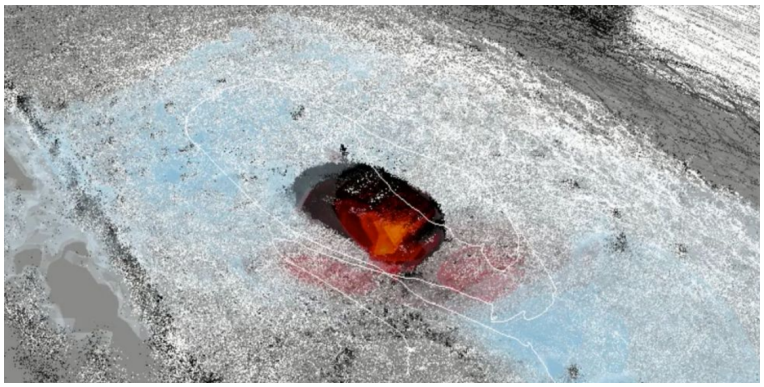

Figure 1. A gray-scale point cloud produced by the NG-LAMP system upon surveying a minivan with a shielded Pu surrogate source in the trunk. The trajectory of NG-LAMP is shown in white and two solutions to Eq. 1 are shown, separately rendered in the blue and red color scales. The blue color scale corresponds to a reconstruction of gamma activity and the red to thermal neutron emission. Whereas the ML-EM algorithm found no particular portion of the point having high gamma emissivity, the trunk area of the minivan was identified as strongly emitting neutrons.

operator of Polaris-LAMP had begun this measurement it was assumed that the heightened gamma-activity in the area was due to that glove box, rather than being emitted from the outlet pipes. The real-time spatially-integrated feedback that SDF enables significantly helped locate this unanticipated material hold-up. Despite its utility, the image overlay remained somewhat rudimentary at that time. Researchers at UC Berkeley have since been developing new user interface capabilities for SDF that leverage virtual reality.[17]

3. SDF ALGORITHM DEVELOPMENTS

The examples presented in the previous section leveraged the ML-EM algorithm to solve formulations of Eq. 1 and did not leverage measurements of the energy-dependent angular detection efficiency $\epsilon(\Omega)$. LBNL has begun characterizing LAMP systems to better enable quantitative SDF solutions. However, free-moving measurements wherein good spatial fidelity is desired (and therefore small voxel sizes) often result in the system matrix being under-determined, or at least rank-deficient. One way to mitigate this shortcoming is to assume sparsity. Foremost, if point-like sources are assumed Hellfeld et al. developed *point source likelihood* (PSL) algorithms to find the most probable source position and activity within a SDF scene atop a constant ambient background.[18] The algorithm also calculates two confidence intervals in real-time. The first uses a likelihood ratio test for the source to be located within any one of the other voxels within the environment, producing a spatial confidence interval and the other considers the counting statistics and the spatial confidence interval to produce an activity confidence interval. The PSL algorithm was subsequently demonstrated in Vavrek et al.[4] and is now the subject of some developments described in Section 4.

One shortcoming of the PSL algorithms is that they were formulated to assume a fixed mean background rate. In small detectors, this may not be problematic, but LBNL researchers are also using the SDF algorithm framework with larger detector arrays such as RadMAP[19] to assess whether context can be used to better estimate how backgrounds change in urban environments. It was first demonstrated that video imagery can correlate with radioactive measurements,[20] and this concept was further developed in Salathe et al.,[21] wherein spectral components of the background were estimated using the RadMAP NaI detector measurements and a semantically-labeled 3D representation of the measured environment.

SDF has also traditionally ignored attenuation due to solid objects within a measured environment and instead calculated the radiation current being emitted from the measured surfaces in a scene. However, Bandstra et al. demonstrated that the PSL algorithm can be reformulated with additional free parameters (such as material attenuation coefficients) to significantly improve localization and activity estimates of sources within obstructing volumes.[22]

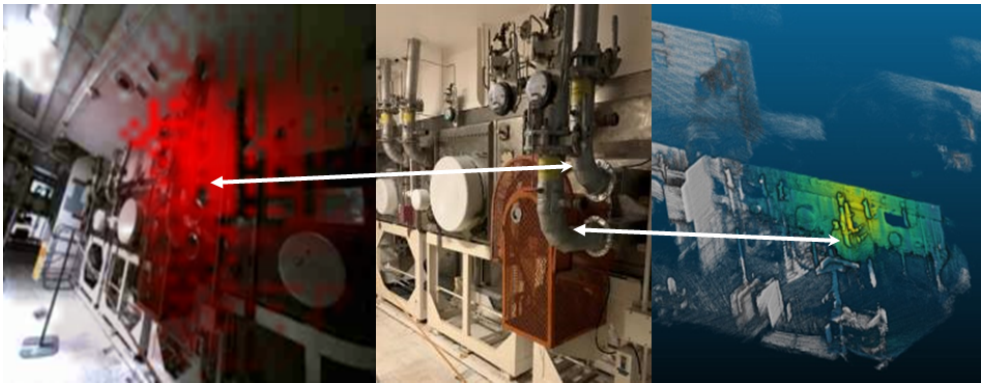

Figure 2. (Left) Screen capture of Polaris LAMP's real-time video overlay showing an appreciable activity on the back side of the glove box. (Middle) photograph of the measured area. (Right) SDF ML-EM Compton imaging data product associating the majority of the measured activity with the upper pipe in the photograph. This pipe had a sticker label that indicated it was an exhaust outlet. The wite arrows are present to help readers orient themselves across the three images.

The ability to localize sources that SDF has demonstrated also inspired the question of how well *should* algorithms perform in a given survey. To address that question, LBNL has recently developed a minimum detectable activity (MDA) estimator algorithm that determines the statistical probability that a radioactive source should be observable, given a well-characterized $\epsilon(\Omega)$, observed background, and the SLAM-derived configuration of the measurement. Using this information, the MDA estimator determines the activity emitted from each voxel that should result in a pre-specified probability of detection using the PSL algorithm.[23]

Beyond the PSL algorithm, LBNL continues to work toward more accurate, more stable, and better quantified SDF algorithms for non point-like distributions of radioactivity. It was recently demonstrated that the ML-EM approach, coupled with regularizer terms (to help induce a more sparse activity map) can render quantitative SDF results in free-moving survey configurations.[5] Additionally, benchmarking data that is summarized in Vavrek's 2022 paper was collected to facilitate development of error estimation algorithms for distributed sources.[24]

4. APPLICATIONS AND OUTLOOK

The advent of quantitative SDF algorithms has allowed researchers to consider autonomous robots that leverage quantitative SDF information as part of their navigation planning. The first example leveraging such a concept has only recently been tested, where a LAMP system operating the PSL algorithm has been configured to control a sUAS that carries it during flight. If the sUAS-LAMP system flies close enough to a radioactive source, the PSL algorithm estimates a source activity confidence interval that is entirely greater than zero. At this point whatever pre-programmed survey pattern (e.g., a raster) the LAMP UAS system was following is interrupted and LAMP instead attempts to localize that source before continuing the mission. To do this, LAMP issues a command to fly toward the point a fixed elevation above the most-probable source position as determined by the PSL algorithm. During this navigation, the PSL algorithm continuously updates and LAMP corresponding continues to updated the way-point for the sUAS to navigate towards. It was observed that intentional modulation of the signal intensity provides the most accurate and precise localization. Therefore, once the most probable source position has become stable for a preset duration (e.g., 5 s), LAMP would issue commands to fly an 'x' pattern above that identified position.

Figure 3 comprises a series of top-down PSL confidence intervals captured on the LAMP UI during one of the first implementations of this type of survey. Here, a LAMP consisting of two Kromex Sigma50 radiation detectors* (called MiniLAMP) flew at an altitude of 13 m above level ground and located a 1 mCi ^{137}Cs source

*It should be noted that the calibration of the two detectors were not of interest prior to these test and it was observed that the two detectors' calibrations differed by several 10's of keV, resulting in an inaccurate and biased $\epsilon(\Omega)$, which we expect caused more erroneous PSL solutions that are typically observed.

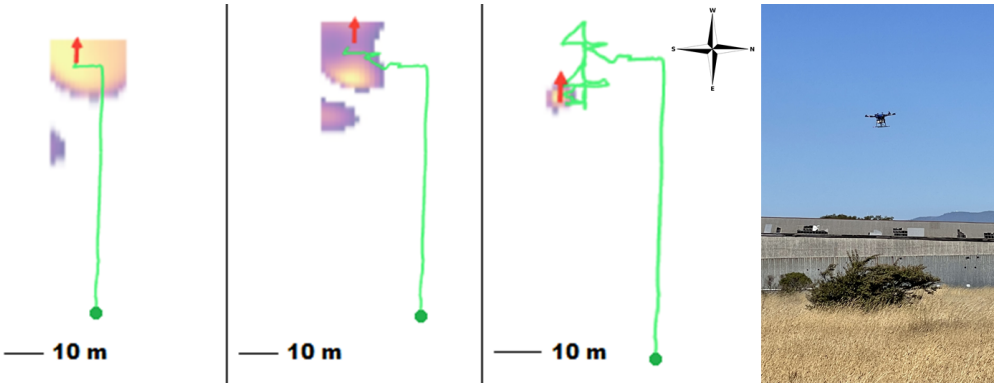

Figure 3. A series of screen captures of the LAMP user interface's top-down view showing PSL confidence intervals view during an autonomous flight and a photograph from the flight. On each screen capture, the dark-green circle indicates the start point, the red arrow indicates the position and heading of the sUAV during the flight, the lighter green indicates the accrued trajectory, and the purple to yellow color scale spans a 5 z-score confidence interval. The left-most image is the first UI view after PSL had determined a source was present, at the time of the second image, the algorithm had been incorrectly biasing the source location wast of the trajectory, and the third image shows the algorithm having correctly located the source position to within a pixel size. Note the zoom level was changed slightly before the right-most image was captured.

set on the ground. The preprogrammed flight occurred at a nominal airspeed of 5 m/s and began by a takeoff and then navigation to the first waypoint that took MiniLAMP west 10 m past the source position along a trajectory that was approximately 20 m north of the source position. The left-most image in Figure 3 is showing the moment shortly after reaching the first way-point and turning south, when the PSL algorithm began to indicate with sufficient confidence that a source was present. At that point, MiniLAMP began issuing commands for the sUAS fly to way-points above the PSL-determined location of highest likelihood, which was incorrectly determined at first to be west of the flight line. The middle image in Figure 3 occurs approximately 10s later and is showing the moment when the PSL algorithm begins determining that the source is in fact east of the current location, however the program had already reached the logical point to begin the 'x' pattern. Upon completion of the first 'x', the UAS is directed to fly further east and perform a second 'x', at which point the source is correctly localized to an accuracy of the pixel size (2 m) and MiniLAMP instructs the UAS to resume its pre-programmed survey.

Having developed an autonomous robotic control algorithm that leverages SDF, we now intend to explore leveraging the MDA mapping algorithm to better perform autonomous radiological search. We have also begun to conceive of means by which semantic segmentation could be performed on LAMP camera feeds to identify objects of radiological interest, which a LAMP could then instruct the robot to approach and enable the LAMP to conduct a form of autonomous inspection.

Beyond the radiological source search problem, we envision SDF-enable autonomy will facilitate:

- mapping for contamination avoidance and/or dose reduction in scenarios following intentional or unintentional radiological dispersion;
- mapping of environmental radioactive contamination to facilitate remediation and long-term management of legacy nuclear sites;
- nuclear facilities inspection for nuclear safeguards, nuclear treaty compliance verification, and to facilitate nuclear operations by identifying material hold-up or spills.

Improving and customizing SDF algorithms and interfaces for these applications, in addition to continued improvement of LAMP hardware are the current focuses of LBNL SDF research and development.

Acknowledgments

This work was performed under the auspices of the U.S. Department of Energy by Lawrence Berkeley National Laboratory under Contract DE-AC02-05CH11231. Aspects of the work summarized here were funded by the U.S. Department of Energy, National Nuclear Security Administration (NNSA) and Offices of Defense Nuclear Nonproliferation Research and Development (DNN R&D) and International Nuclear Safeguards. Previously published work supported by the U.S. Department of Defence, Defense Threat Reduction Agencency Nuclear Detection Division (DTRA-NTD) was also summarized. Some of this research used resources of the National Energy Research Scientific Computing Center (NERSC), a U.S. Department of Energy Office of Science User Facility operated under Contract No. DE-AC02-05CH11231.

REFERENCES

[1] Barnowski, R., Haefner, A., Mihailescu, L., and Vetter, K., "Scene data fusion: Real-time standoff volumetric gamma-ray imaging," *Nuclear Instruments and Methods in Physics Research Section A: Accelerators, Spectrometers, Detectors and Associated Equipment* **800**, 65–69 (2015).

[2] Haefner, A., Barnowski, R., Luke, P., Amman, M., and Vetter, K., "Handheld real-time volumetric 3-d gamma-ray imaging," *Nuclear Instruments and Methods in Physics Research Section A: Accelerators, Spectrometers, Detectors and Associated Equipment* **857**, 42–49 (2017).

[3] Vetter, K., Barnowski, R., Cates, J. W., Haefner, A., Joshi, T. H., Pavlovsky, R., and Quiter, B. J., "Advances in nuclear radiation sensing: Enabling 3-d gamma-ray vision," *Sensors* **19**(11), 2541 (2019).

[4] Vavrek, J. R., Hellfeld, D., Bandstra, M. S., Negut, V., Meehan, K., Vanderlip, W. J., Cates, J. W., Pavlovsky, R., Quiter, B. J., Cooper, R. J., and Joshi, T. H. Y., "Reconstructing the position and intensity of multiple gamma-ray point sources with a sparse parametric algorithm," *IEEE Transactions on Nuclear Science* **67**(11), 2421–2430 (2020).

[5] Hellfeld, D., Bandstra, M. S., Vavrek, J. R., Gunter, D. L., Curtis, J. C., Salathe, M., Pavlovsky, R., Negut, V., Barton, P. J., Cates, J. W., et al., "Free-moving quantitative gamma-ray imaging," *Scientific reports* **11**(1), 1–14 (2021).

[6] Vetter, K., Barton, P., Barnowski, R., Cates, J., Haefner, A., Joshi, T., Pavlovsky, R., and Quiter, B., "3d gamma-ray imaging and real-time visualization from freely moving platforms (conference presentation)," in [*Hard X-Ray, Gamma-Ray, and Neutron Detector Physics XXI*], James, R. B., Burger, A., and Payne, S. A., eds., **11114**, 1111402, International Society for Optics and Photonics, SPIE (2019).

[7] Pavlovsky, R., Cates, J., Vanderlip, W., Joshi, T., Haefner, A., Suzuki, E., Barnowski, R., Negut, V., Moran, A., Vetter, K., et al., "3d gamma-ray and neutron mapping in real-time with the localization and mapping platform from unmanned aerial systems and man-portable configurations," *arXiv preprint arXiv:1908.06114* (2019).

[8] Joshi, T., Quiter, B., Bandstra, M., Pavlovsky, R., Hellfeld, D., Moran, A., Cates, J., Vavrek, J., Agency, D. D. T. R., and USDOE, "Localization and mapping platform software (lamp) v3," (3 2018).

[9] Hess, W., Kohler, D., Rapp, H., and Andor, D., "Real-time loop closure in 2d lidar slam," in [*2016 IEEE international conference on robotics and automation (ICRA)*], 1271–1278, IEEE (2016).

[10] Joshi, T. H. Y., Quiter, B. J., Maltz, J. S., Bandstra, M. S., Haefner, A., Eikmeier, N., Wagner, E., Luke, T., Malchow, R., and McCall, K., "Measurement of the energy-dependent angular response of the ares detector system and application to aerial imaging," *IEEE Transactions on Nuclear Science* **64**(7), 1754–1760 (2017).

[11] Shirwadkar, U., Hawrami, R., Glodo, J., Van Loef, E., and Shah, K., "Novel scintillation material cs 2 lilabr 6- x cl x: Ce for gamma-ray and neutron spectroscopy," in [*2012 IEEE Nuclear Science Symposium and Medical Imaging Conference Record (NSS/MIC)*], 1963–1967, IEEE (2012).

[12] Guss, P. P., Stampahar, T. G., Mukhopadhyay, S., Barzilov, A., and Guckes, A., "Scintillation properties of a cs2lila (br6) 90%(cl6) 10%: Ce3+ (cllbc) crystal," in [*Radiation Detectors: Systems and Applications XV*], **9215**, 27–41, SPIE (2014).

[13] Hecla, J., Knecht, K., Gunter, D., Haefner, A., Hellfeld, D., Joshi, T. H. Y., Moran, A., Negut, V., Pavlovsky, R., and Vetter, K., "Polaris-lamp: Multi-modal 3-d image reconstruction with a commercial gamma-ray imager," *IEEE Transactions on Nuclear Science* **68**(10), 2539–2549 (2021).

[14] Wahl, C. G., Kaye, W. R., Wang, W., Zhang, F., Jaworski, J. M., King, A., Boucher, Y. A., and He, Z., "The polaris-h imaging spectrometer," *Nuclear Instruments and Methods in Physics Research Section A: Accelerators, Spectrometers, Detectors and Associated Equipment* **784**, 377–381 (2015).

[15] Knecht, K., Hellfeld, D., Pavlovsky, R., Quiter, B., Joshi, T. H. Y., Torii, T., Furuta, Y., and Vetter, K., "Evaluating 3d gamma-ray imaging techniques for distributed sources at the fukushima daiichi nuclear power station," in [*2020 IEEE Nuclear Science Symposium and Medical Imaging Conference (NSS/MIC)*], 1–5 (2020).

[16] "Plutonium-238 production for space exploration." https://www.acs.org/content/dam/acsorg/education/whatischemistry/landmarks/plutonium-238-production/plutonium-238-booklet.pdf. Accessed: 2022-08-19.

[17] Dayani, P., Orr, N., Saran, V., Hu, N., Krishnaswamy, S., Thomopoulos, A., Wang, E., Bae, J., Zhang, E., McPherson, D., Menke, J., Moran, A., Quiter, B., Yang, A., and Vetter, K., "Immersive operation of a semi-autonomous aerial platform for detecting and mapping radiation," *IEEE Transactions on Nuclear Science* **68**(12), 2702–2710 (2021).

[18] Hellfeld, D., Joshi, T. H. Y., Bandstra, M. S., Cooper, R. J., Quiter, B. J., and Vetter, K., "Gamma-ray point-source localization and sparse image reconstruction using poisson likelihood," *IEEE Transactions on Nuclear Science* **66**(9), 2088–2099 (2019).

[19] Bandstra, M. S., Aucott, T. J., Brubaker, E., Chivers, D. H., Cooper, R. J., Curtis, J. C., Davis, J. R., Joshi, T. H., Kua, J., Meyer, R., et al., "Radmap: The radiological multi-sensor analysis platform," *Nuclear Instruments and Methods in Physics Research Section A: Accelerators, Spectrometers, Detectors and Associated Equipment* **840**, 59–68 (2016).

[20] Bandstra, M. S., Quiter, B. J., Curtis, J. C., Bilton, K. J., Joshi, T. H., Meyer, R., Negut, V., Vetter, K., Archer, D. E., Hornback, D. E., Peplow, D. E., Romano, C. E., Swinney, M. W., McCullough, T. L., and McLean, M. L., "Attribution of gamma-ray background collected by a mobile detector system to its surroundings using panoramic video," *Nuclear Instruments and Methods in Physics Research Section A: Accelerators, Spectrometers, Detectors and Associated Equipment* **954**, 161126 (2020). Symposium on Radiation Measurements and Applications XVII.

[21] Salathe, M., Quiter, B. J., Bandstra, M. S., Curtis, J. C., Meyer, R., and Chow, C. H., "Determining urban material activities with a vehicle-based multi-sensor system," *Phys. Rev. Research* **3**, 023070 (Apr 2021).

[22] Bandstra, M. S., Hellfeld, D., Vavrek, J. R., Quiter, B. J., Meehan, K., Barton, P. J., Cates, J. W., Moran, A., Negut, V., Pavlovsky, R., and Joshi, T. H. Y., "Improved gamma-ray point source quantification in three dimensions by modeling attenuation in the scene," *IEEE Transactions on Nuclear Science* **68**(11), 2637–2646 (2021).

[23] Bandstra, M. S., Hellfeld, D., Lee, J., Quiter, B. J., Salathe, M., Vavrek, J. R., and Joshi, T. H., "Mapping the minimum detectable activities of gamma-ray sources in a 3-d scene," *arXiv preprint arXiv:2208.03321* (2022).

[24] Vavrek, J. R., Hines, C. C., Bandstra, M. S., Hellfeld, D., Heine, M. A., Heiden, Z. M., Mann, N. R., Quiter, B. J., and Joshi, T. H., "Design and deployment of radiological point-source arrays for the emulation of continuous distributed sources," *arXiv preprint arXiv:2208.02899* (2022).